

NASA/TM—1998-208490



Excitation of Continuous and Discrete Modes in Incompressible Boundary Layers

David E. Ashpis
Lewis Research Center, Cleveland, Ohio

Eli Reshotko
Case Western Reserve University, Cleveland, Ohio

National Aeronautics and
Space Administration

Lewis Research Center

July 1998

Trade names or manufacturers' names are used in this report for identification only. This usage does not constitute an official endorsement, either expressed or implied, by the National Aeronautics and Space Administration.

Available from

NASA Center for Aerospace Information
7121 Standard Drive
Hanover, MD 21076
Price Code: A04

National Technical Information Service
5287 Port Royal Road
Springfield, VA 22100
Price Code: A04

**EXCITATION OF CONTINUOUS AND DISCRETE MODES
IN INCOMPRESSIBLE BOUNDARY LAYERS**

David E. Ashpis

NASA Lewis Research Center
Cleveland, Ohio 44135

and

Eli Reshotko

Department of Mechanical and Aerospace Engineering
Case Western Reserve University
Cleveland, Ohio 44106

ABSTRACT

This report documents the full details of the condensed journal article by Ashpis & Reshotko (JFM, 1990) entitled "The Vibrating Ribbon Problem Revisited". A revised formal solution of the vibrating ribbon problem of hydrodynamic stability is presented. The initial formulation of Gaster (JFM, 1965) is modified by application of the Briggs method and a careful treatment of the complex double Fourier transform inversions. Expressions are obtained in a natural way for the discrete spectrum as well as for the four branches of the continuous spectra. These correspond to discrete and branch-cut singularities in the complex wave-number plane. The solutions from the continuous spectra decay both upstream and downstream of the ribbon, with the decay in the upstream direction being much more rapid than that in the downstream direction. Comments and clarification of related prior work are made.

. Preface

This report documents the full details of the concise article entitled "The Vibrating Ribbon Problem Revisited" by Ashpis & Reshotko which appeared in the Journal of Fluid Mechanics (1990), vol. 213, pp. 531-547. This report constitutes the full manuscript that was originally submitted for publication, but had to be shortened and condensed due to space limitations. It is based on Ashpis & Reshotko (1986), a work principally supported by the US Air Force Office of Scientific Research. The present report was written after the first author joined NASA. Some typographical errors of the prior work were corrected and comments of the journal reviewers were implemented. There has been recently renewed interest in the continuous spectrum in context of its relationship to the new concepts of transient growth in hydrodynamic stability theory and its role in receptivity to freestream disturbances. Therefore it was felt that the details and the structure of this report make its documentation in form of a NASA report a valuable complement to the journal article and an accessible text to non-specialists.

1. Introduction

The vibrating ribbon became a common experimental device in hydrodynamic stability research since its first use by Schubauer and Skramstad (1947) to excite TS waves in boundary layer flow. The importance of this fundamental device goes beyond this practical application. The vibrating ribbon problem serves as a simple example of receptivity problems, which express the effect of imposed disturbances on the flow, and are significant in describing the onset of instabilities leading to transition from laminar to turbulent flow.

This problem, also known as the signaling problem, was initially treated by Gaster (1965), whose analysis verified Schubauer and Skramstad's observation that in the time-asymptotic (long time) limit the ribbon excites the spatial eigenmodes of the flow at its own frequency. Additional analytical work is reported in Russian literature (e.g. Tumin and Federov, 1984). In free shear layers the signaling problem was treated by Huerre & Monkewitz (1985) for the inviscid case. We found Gaster's solution incomplete. Mainly missing are the continuous spectra. Therefore we provide here a corrected and complete solution.

Gaster's initial formulation of the problem is followed: the model, the formulation as an IBVP (Initial Boundary Value Problem), and the application of a double Fourier transform (or Laplace-Fourier transform), are essentially similar, but we proceed with a different solution procedure. We use the Briggs method (Briggs, 1964) to obtain the time-asymptotic solution. Common for long time in plasma physics (see review by Bers, 1983), this method was first used in fluid mechanics by Tam (1971, 1978). It became more established in this field following a large number of its applications in later years. For example it was used by Huerre & Monkewitz (1985), Ashpis & Reshotko (1985), Leib & Goldstein (1986), Pierrehumbert (1986), Monkewitz & Sohn (1986), Hultgren & Aggarwal (1987), Monkewitz (1988), Lin & Lian (1989), Yang & Zebib (1989), and was reviewed by Huerre (1987). The Briggs method requires an accurate account of the

singularities in the transformed planes which is performed here in a methodical way. As a result the continuous spectra are included in our solution, and various related topics are illuminated.

The continuous spectra were addressed by Case (1960, 1961) [†]. A comprehensive treatment was given by Grosch & Salwen (1978) and Salwen & Grosch (1981), who extended the classical normal mode formulation. They identified the one branch of continuous spectra in the temporal case, and the four branches in the spatial case, but left unsettled a difficulty in the physical interpretation of two of the branches in the spatial case.

Continuous spectra were obtained also in formulations of linear stability problems as IVP (Initial Value Problem) and IBVP: When solved by Fourier or Laplace Transform methods, the continuous spectra emerge from branch-cuts in the complex transform planes. The temporal continuous spectrum was obtained by Gustavsson (1979) who formulated an IVP. His work was used by Salwen & Grosch (1981) to prove completeness of the temporal eigenfunction expansion. Tsuge & Rogler (1983) treated a forced problem formulated as IBVP and obtained two branches of the spatial continuous spectra, but dismissed one of them as nonphysical. They ignored an inconsistency in their solution, which yielded a branch-cut singularity in a region of the complex transformed plane that should be analytic. The same branches were obtained also by Aldoss (1982). A similar forced problem for compressible flow was also treated as an IBVP by Tumin & Fedorov (1983), who found seven branches of the spatial continuous spectra. They recognize the same inconsistency, proposed a method to resolve the difficulty, but which does not seem to be a practical one.

In the solution here presented, the continuous spectra emerge in a natural way as part of the complete solution and the solution is mathematically consistent. The solution

[†] After completion of this manuscript the authors have found that the continuous spectra was also addressed by Murdock & Stewartson (1977) and Hultgren & Gustavsson (1981).

procedure is applicable to a wider class of problems, and clarifies the prior difficulties.

The outline of this work is as follows: The problem is formulated in Section 2 and the solution in the transformed domain is presented in Section 3. Reference is made to necessary details which are given in Appendices A and B. The inversion to the physical domain is performed in Section 4, which includes description of the singularities and the application of the Briggs method. The physical meaning of the results is described in Section 5. The discussion in Section 6 includes a comparison to Gaster (1965), and comments about related topics. It is found necessary to include an outline of Gaster's solution in Appendix C in order to simplify the comparison. The present work is based on unpublished work by the authors, Ashpis & Reshotko (1985,1986), where further detail can be found.

2. Formulation of the problem

The physical problem is modeled as shown in Figure 1. Two-dimensional incompressible boundary layer flow over a flat plate is assumed, and the ribbon is modeled as a line source of disturbances imbedded at the wall at the origin O of the cartesian coordinates x, y . The longitudinal and normal velocity components are U and V , respectively, and the freestream velocity is U_∞ . We are interested in the response of the boundary layer to two-dimensional harmonic excitation of the ribbon starting at $t = 0$.

The assumption is that the vibrations of the ribbon are infinitesimally small, justifying use of linear stability theory. The velocity is split into basic (\bar{U}, \bar{V}) and disturbed (u, v) parts, and the standard procedures of linear stability theory are applied. Assuming parallel flow, $\bar{V} = 0$, $\bar{U} = \bar{U}(y)$, the nondimensional equation for the normal disturbance velocity v is

$$\left[\frac{\partial}{\partial t} + \bar{U} \frac{\partial}{\partial x} \right] \nabla^2 v - \bar{U}'' \frac{\partial v}{\partial x} = \frac{1}{R} \nabla^4 v \quad (1)$$

where R is the Reynolds number based on U_∞ and on the displacement thickness δ^* , $\bar{U}'' = \frac{d^2 \bar{U}(y)}{dy^2}$, $\nabla^2 = \frac{\partial^2}{\partial x^2} + \frac{\partial^2}{\partial y^2}$, and $v = v(y; x, t)$. The independent variables are used in the order $y; x, t$ throughout this paper for convenience.

The effect of the ribbon is formulated as a wall boundary condition on the normal velocity

$$v(0; x, t) = \cos \omega_0 t \delta(x) H(t) \quad (2a)$$

where ω_0 is the real frequency of vibration of the ribbon, δ is Dirac's Delta function, which expresses the modelling of the ribbon as a line disturbance, and $H(t)$ is the unit step function, which indicates that the motion starts from rest at $t = 0$. The second boundary condition at the wall, from continuity, is

$$\frac{\partial v(0; x, t)}{\partial y} = 0 \quad (2b)$$

As $y \rightarrow \infty$ it is required that

$$v(y; x, t) \Big|_{y \rightarrow \infty} \rightarrow 0 \quad (3a)$$

$$\frac{\partial v(y; x, t)}{\partial y} \Big|_{y \rightarrow \infty} \rightarrow 0 \quad (3b)$$

We use the generalized double Fourier transform defined as

$$\Phi(y; \alpha, \omega) = \int_{-\infty}^{\infty} dt \int_{-\infty}^{\infty} dx v(y; x, t) e^{-i(\alpha x - \omega t)} \quad (4)$$

where α is the complex wave number and ω is the complex frequency. The lower limit of the time integration can be replaced by 0, because v is a causal function in t ($v = 0$ for $t < 0$). The Fourier transform on time is then identical to the Laplace transform on time, with the transform variable S related to ω by the relation $S = -i\omega$. Thus (4) may also be referred to as a Laplace-Fourier transform.

Transforming Equation (1) yields the Orr-Sommerfeld equation

$$\{(D^2 - \alpha^2)(D^2 - \hat{\mu}^2) + i\alpha R \bar{U}''\} \{\Phi\} = 0 \quad (5)$$

where

$$\hat{\mu}^2 = \alpha^2 + i\alpha R \left[\bar{U}(y) - \frac{\omega}{\alpha} \right] \quad (6)$$

$$D \equiv \frac{d}{dy}$$

$$\Phi \equiv \Phi(y; \alpha, \omega)$$

Φ is considered a function of y , with α and ω as parameters. R is also a parameter, but omitted from the list of independent variables throughout this paper.

Transformation of (2), the boundary conditions at the wall ($y = 0$), yields

$$\Phi(0; \alpha, \omega) = \frac{i\omega}{\omega^2 - \omega_0^2} \quad (7a)$$

$$\frac{\partial \Phi(0; \alpha, \omega)}{\partial y} = 0 \quad (7b)$$

Transforming (3), the boundary conditions as $y \rightarrow \infty$, results in the requirements

$$\Phi(y; \alpha, \omega) \Big|_{y \rightarrow \infty} \rightarrow 0 \quad (8a)$$

$$\frac{\partial \Phi(y; \alpha, \omega)}{\partial y} \Big|_{y \rightarrow \infty} \rightarrow 0 \quad (8b)$$

Equations (5) to (8) form a non-homogeneous system, where the nonhomogeneity appears in the boundary condition (7a).

The solution of the equation is

$$\Phi = \sum_{j=1}^4 C_j \Phi_j \quad (9)$$

where $\Phi_j \equiv \Phi_j(y; \alpha, \omega)$, ($j = 1, \dots, 4$), are the four fundamental solutions of the Orr-Sommerfeld equation. $C_j \equiv C_j(\alpha, \omega)$ are constants with respect to y , to be determined by applying the boundary conditions.

The outline of the formulation to this point is similar to Gaster's (1965), except that the latter is done in terms of the disturbance stream function (see Appendix C and Section 6).

3. Solution in the transformed domain

The fundamental solutions of the Orr-Sommerfeld equation need to be used in order to find the constants C_j from the boundary conditions. However, exact closed-form solutions of the equation for a general profile $\bar{U}(y)$ are not known, except for its asymptotic solutions as $y \rightarrow \infty$. These solutions will be used when applying the boundary conditions (8), and Φ will then be expressed in terms of the fundamental solutions and their derivatives at the wall as follows.

3.1. Asymptotic solutions of the Orr-Sommerfeld equation as $y \rightarrow \infty$

As $y \rightarrow \infty$, $\bar{U} \rightarrow U_\infty$ and $\bar{U}'' \rightarrow 0$. Taking $\bar{U}_\infty = 1$, the Orr-Sommerfeld equation (5) takes the form

$$\{(D^2 - \alpha^2)(D^2 - \mu^2)\}\{\tilde{\Phi}\} = 0 \quad (10)$$

where

$$\mu^2 = \alpha^2 + iR(\alpha - \omega) \quad (11)$$

and

$$\tilde{\Phi}_j = \Phi_j|_{y \rightarrow \infty} \quad (12)$$

$$\mu^2 = \hat{\mu}^2|_{y \rightarrow \infty} \quad (123)$$

Equation (10) is the asymptotic form as $y \rightarrow \infty$ of the Orr-Sommerfeld equation, and can be solved exactly. Its four solutions $\tilde{\Phi}_j$ are the asymptotic forms as $y \rightarrow \infty$ of the four solutions Φ_j of (5), and are of the exponential form

$$\tilde{\Phi}_j = e^{r_j y} \quad (j = 1, \dots, 4) \quad (14)$$

where r_j are the four solutions of the characteristic equation

$$(r^2 - \alpha^2)(r^2 - \mu^2) = 0 \quad (15)$$

Let r_1 and r_3 be the solutions of $r^2 - \mu^2 = 0$, and r_2 and r_4 be the solutions of $r^2 - \alpha^2 = 0$. Therefore solving for the r_j 's requires taking the square root of the complex functions α^2 and μ^2 . To emphasize this point, we write r_j as

$$r_{3,1} = \pm(\mu^2)^{1/2} \quad (16)$$

$$r_{4,2} = \pm(\alpha^2)^{1/2} \quad (17)$$

Evaluation of the complex square root requires compliance with a convention for making the square root function single valued, and construction of branch-cuts in the α and ω planes. It seems that this point, although elementary, has been somewhat overlooked in prior work. The evaluation is detailed in Appendix A, where use of a mapping to an auxiliary plane yields clear definitions of the branch-cuts and a demonstration of their properties. It is shown there that

$$r_{3,1} = \pm\mu \quad (18)$$

where μ is the complex square root of (11), properly defined as a single valued function by the convention specified in Appendix A.

The function μ depends on the three parameters α , ω , and R . As shown in Appendix A, at fixed ω and R , the branch-cuts for μ in the α -plane take the form of two hyperbola sections (Figures 2b and 6). In the ω -plane, at fixed α and R , the branch-cut for μ is a straight line section (Figures 2a and 7). The choice of the branch-cuts in either case ensures that

$$\text{Real}(\mu) > 0 \quad \text{for all } \alpha \text{ and } \omega \quad (19)$$

This property will be exploited when applying the boundary conditions.

To assist in the evaluation of $r_{4,2}$, we define the function ζ as

$$\zeta = [(\alpha - i\varepsilon)(\alpha + i\varepsilon)]^{1/2} \quad (20)$$

where the convention for the complex square root function is in effect. It is shown in

Appendix A that

$$r_{4,2} = \pm \lim_{\varepsilon \rightarrow 0} \zeta \quad (21)$$

Let

$$\alpha = \alpha_r + i\alpha_i \quad (22)$$

where the subscript r indicates the real part of α , and i indicates its imaginary part. This notation applies also to other complex variables throughout this paper. Then (21) can also be written as

$$r_{4,2} = \pm \text{sign}(\alpha_r) \cdot \alpha \quad (23)$$

The branch-cuts which make ζ single valued are sections of the imaginary α -axis, from the branch-points $\pm i\varepsilon$ to $\pm i\infty$ (Figures 2b and 8). As $\varepsilon \rightarrow 0$ the branch-points approach the origin, and the branch-cuts span the whole imaginary α -axis, excluding the point of origin $\alpha = 0$, which stays a regular point. By the choice of these branch-cuts it is ensured that

$$\text{Real}(\zeta) > 0 \quad \text{for all } \alpha \quad (24)$$

This property will also be exploited when applying the boundary conditions.

The asymptotic solutions are obtained by inserting r_j from (18) and (21) into (14),

$$\tilde{\Phi}_1 = e^{-\mu y} \quad (25a)$$

$$\tilde{\Phi}_3 = e^{+\mu y} \quad (25b)$$

$$\tilde{\Phi}_2 = \lim_{\varepsilon \rightarrow 0} e^{-\zeta y} \quad (25c)$$

$$\tilde{\Phi}_4 = \lim_{\varepsilon \rightarrow 0} e^{+\zeta y} \quad (25d)$$

3.2. Application of the Boundary Conditions

To apply the boundary conditions at $y \rightarrow \infty$ let $\mu = \mu_r + i\mu_i$ and write (25b) as

$$\tilde{\Phi}_3 = e^{\mu_r y} e^{i\mu_i y} \quad (26)$$

The second exponential in (26) represents a pure oscillation, and the first is its amplitude modifier. Since $y > 0$, growth or decay are determined by the sign of μ_r . Since $\mu_r > 0$ for all α and ω , as follows from (19), the solution $\tilde{\Phi}_3$ is unbounded as $y \rightarrow \infty$, requiring $C_3 = 0$. By using a similar argument, following (24), it is concluded that $\tilde{\Phi}_1$ is unbounded as $y \rightarrow \infty$, requiring $C_4 = 0$. $\tilde{\Phi}_1$ and $\tilde{\Phi}_2$ decay as $y \rightarrow \infty$, therefore Φ_1 and Φ_2 are acceptable solutions.

The two remaining constants C_1 and C_2 are determined by applying the boundary conditions (8) at the wall. The result for Φ is

$$\Phi \equiv \Phi(y; \alpha, \omega) = \frac{i\omega}{\omega^2 - \omega_0^2} \frac{\Delta}{\Delta_0} \quad (27)$$

where

$$\Delta \equiv \Delta(y; \alpha, \omega) = \Phi_1 \Phi'_{20} - \Phi'_{10} \Phi_2 \quad (28a)$$

$$\Delta_0 \equiv \Delta(0; \alpha, \omega) = \Phi_{10} \Phi'_{20} - \Phi'_{10} \Phi_{20} \quad (\Delta \text{ at } y = 0) \quad (28b)$$

$$\Phi_j \equiv \Phi_j(y; \alpha, \omega) \quad (j = 1, 2) \quad (28c)$$

$$\Phi_{j0} \equiv \Phi_j(0; \alpha, \omega) \quad (j = 1, 2) \quad (\Phi_j \text{ at } y = 0) \quad (28d)$$

$$(\)' \equiv \frac{d}{dy} \quad (28e)$$

It is important to emphasize the role of the particular choice of branch-cuts in this process. If different branch-cuts would have been constructed, then the growth and decay of the solutions as $y \rightarrow \infty$ would depend on subdomains in the α and ω planes, making the solution more complicated, if not impossible.

4. Inversion to the physical domain

4.1. The singularities of Φ

The function Φ possesses continuous and discrete singularities which are important for the inversion to the physical domain. The continuous singularities are the branch-cuts in the complex α and ω planes which are discussed in Section 3.1 above and in Appendix A. The discrete singularities are the zeroes of the two terms in the denominator of (27): (i) The zeroes of $(\omega^2 - \omega_0^2)$ yield two poles at $\omega = \pm\omega_0$ along the real axis of the ω -plane; and (ii) the zeroes of Δ_0 yield additional poles in both the ω -plane and in the α -plane. These latter pole singularities (ii) are discussed in the remainder of this section.

These discrete singularities (ii) are obtained by solving

$$\Delta_0(\alpha, \omega) = 0 \quad (29)$$

For fixed R the expression (29) yields

$$\alpha = \alpha_j(\omega) \quad (j = 1, \dots, N) \quad (30)$$

The expression (30) represents N ω -dependent poles in the α -plane. As ω varies, the poles trace trajectories there. Alternatively, (29), can be solved for ω to yield

$$\omega = \omega_j(\alpha) \quad (j = 1, \dots, M) \quad (31)$$

which corresponds to M α -dependent poles in the ω -plane, which form trajectories in the ω -plane as α varies.

Both α and ω are complex in the expression (29), which can be considered as the generalized form of the dispersion relations which are obtained in the spatial or temporal normal mode analysis of linear stability theory. The eigenvalues in the spatial formulation are a special case of (30) with real ω , and the eigenvalues in the temporal formulation are a special case of (31) with real α .

A complete description of the discrete singularities is needed in order to perform the inversion. The suitable form of this description are fixed Reynolds-number maps of families of constant ω_i and ω_r trajectories of $\alpha_j(\omega)$ in the α -plane, for all the j modes; or, alternatively, similar maps of constant α_i and α_r trajectories of $\omega_j(\alpha)$ in the ω -plane. It is to be noted that negative frequencies and wave numbers need also to be included. It is, however, sufficient to specify in the α -plane only trajectories of $\alpha_j(\omega)$ for ω 's with positive real frequencies $\omega_r > 0$, because it follows from the symmetry property (B4) (Appendix B) that constant ω_i trajectories of $\alpha_j(\omega)$ for $\omega_r > 0$ are symmetric, with respect to the imaginary α -axis, to the ones for $\omega_r < 0$. Similarly, it follows from (B5) that constant α_i trajectories of $\omega_j(\alpha)$ for $\alpha_r > 0$ are symmetric, with respect to the imaginary ω -axis, to the ones for $\alpha_r < 0$, and it is therefore sufficient to specify in the ω -plane only trajectories of $\omega_j(\alpha)$ for positive wave numbers.

We attempted constructing the required trajectories for boundary layer flow based on data from the open literature, but found that the available data are not sufficient for that purpose. The only reported computations known to us when both α and ω are complex are by Gaster & Jordinson (1975) and Koch (1986). Some trajectories $\alpha_j(\omega)$ can be derived from the data presented in those works, but unfortunately they are limited to negative values of ω_i , a range which is not useful for the present analysis. The rest of the reported computations for boundary layers are of either the spatial or the temporal modes, where either α or ω is pure real. These computations (e. g. Mack (1976)) show that for finite R the number of eigenmodes N and M is finite, and that there is only one unstable mode. The only theoretical proof is by Miklavčič & Williams (1982) and Miklavčič (1983) for the temporal case at finite R . This problem is not addressed here and we assume that N and M are finite. (1982) and Miklavčič (1983) for the temporal case at finite R . The problem of the number of modes is not addressed here and we assume that N and M are finite. For clarity we designate this mode with subscript $j = 1$ and refer to it as the unstable Tollmien-Schlichting (TS) mode. We attach the subscripts

$j = 2, \dots, N$ (or M) to the other modes, and refer to them as the higher, or stable, modes.

Although the TS mode itself has been extensively investigated computationally, there is still lack of sufficient data to obtain the complete trajectory maps even for the spatial and temporal cases, because much less detailed data exist for the higher modes.

It is, however, known that the trajectories of the higher modes $\omega_j(\alpha_r)$ and $\alpha_j(\omega_r)$ ($j = 2, \dots, N$ or M), are in the lower half ω -plane and in the upper half α -plane, respectively, for all R . In comparison, accurate trajectories of $\alpha_1(\omega_r)$ ($\omega_i = 0$), and of $\omega_1(\alpha_r)$ ($\alpha_i = 0$), can be constructed for a wide range of ω_r and α_r , respectively. At $R > R_{cr}$ the trajectory of $\omega_1(\alpha_r)$ crosses the real ω -axis and has a maximum in the upper half ω -plane, and the trajectory of $\alpha_1(\omega_r)$ crosses the real α -axis and has a minimum in the lower half α -plane.

Computation of the generalized trajectories, when both α and ω are complex is beyond the scope of the present work, however, a qualitative investigation of the relative location of these trajectories for the unstable TS mode was performed in Ashpis & Reshotko (1986), based on the known spatial and temporal cases. It is shown there that the constant ω_i trajectory of $\alpha_1(\omega)$ shifts upward with increased ω_i , and is completely above the real α -axis for some positive $\omega_i = \sigma$. Similar qualitative conclusions regarding the trajectories of the higher modes cannot be drawn due to the unavailability of extensive computational results. In particular it is not known if trajectories can coalesce.

Attention needs to be given also to the left-half complex planes, where the poles have negative real parts. The existence of eigenvalues with negative real parts, corresponding to waves moving in the upstream direction, has never been reported in literature. These are spatial eigenvalues $\alpha_j(\omega_r)$, for positive ω_r , corresponding to poles in the left half α -plane, and temporal eigenvalues $\omega_j(\alpha_r)$, for positive α_r , corresponding to poles in the left half ω -plane. It is not clear if researchers have searched the left half-planes for eigenvalues without success, or if this search was not attempted at all. The implication

to the present work is that the existence of trajectories for $\omega_r > 0$ in the left half α -plane, and the existence of trajectories for $\alpha_r > 0$ in the left half ω -plane is unknown.

4.2. Inversion formula

Inversion of Φ to the physical domain is obtained according to the inversion formula

$$v(y; x, t) = \frac{1}{(2\pi)^2} \int_L \int_F \Phi(y; \alpha, \omega) e^{i(\alpha x - \omega t)} d\alpha d\omega \quad (32)$$

where F is the inversion contour in the α -plane, and L is the inversion contour in the ω -plane. The inversion contours lie in the region of analyticity of Φ in the respective planes, as shown in Figure 2, which incorporates results of the discussion of the previous section.

Based on causality, the region of analyticity is an upper half-plane in the ω -plane, with all singularities of Φ lying in the remaining lower half-plane. Therefore L is a line passing above all the singularities of Φ in the ω -plane.

Since v is defined for $-\infty > x > \infty$ there is a strip of analyticity in the α -plane which includes the real α -axis. The strip is confined between $\pm i\varepsilon$, and all of the singularities of Φ are located above and below it. As $\varepsilon \rightarrow 0$ the strip degenerates to the real α -axis, allowed by the fact that the origin remains a regular point. Therefore F can be taken along the real α -axis, conveniently making α in (32) pure real.

The two inversions in (32) are interrelated. It means that if the ω inversion is made first, α serves as a parameter whose value is taken along F . Since F coincides with the real α -axis, the singularities of interest in the ω -plane are the ones for pure real α . The discrete ones are by definition the temporal eigenvalues, and the continuous ones are along the ω 's defined by the straight-line branch-cut for $\alpha = \alpha_r$, as shown in Figure 2a. Since this branch-cut is always below the real ω -axis (Appendix A), L lies in the upper half ω -plane above the maximum point of the temporal TS trajectory $\omega_1(\alpha_r)$ ($\alpha_i = 0$). If L is the line $\omega = i\sigma$, then σ is positive. This conforms to the analyticity properties in the ω -plane which were discussed above. If the α inversion is made first, the interdependence of the two inversions requires the singularities in the α -plane to be taken for values of ω on L , meaning for ω 's with $\omega_i = \sigma$. The previous discussion showed that for these ω 's

the poles are located in the upper half α -plane, and that the branch-cuts do not cross the real α -axis (Appendix A), which conforms to the requirement for existence of a strip of convergence there.

At this point the inversion contours are determined and the inversion according to (32) can, at least in principle, be performed.

4.3. The time-asymptotic form

The present interest is principally in the time-asymptotic form of the solution, v as $t \rightarrow \infty$. For this purpose we apply the method of Briggs (Briggs 1964) (see Section 1). When using this method, the inversion is made first from α to x , to obtain \hat{v} as

$$\hat{v}(y; x, \omega) = \frac{1}{2\pi} \int_F \Phi(y; \alpha, \omega) e^{i\alpha x} d\alpha \quad (33)$$

followed by inverting \hat{v} from ω to t according to

$$v(y; x, t) = \frac{1}{2\pi} \int_L \hat{v}(y; x, \omega) e^{-i\omega t} d\omega \quad (34)$$

The method of Briggs requires deflecting the contour L towards L_1 , which is located slightly below the real ω -axis (Figure 3a). The exponential term in (34) will make the integrand vanish along the straight portions of L_1 as $t \rightarrow \infty$, leaving the time-asymptotic form to be determined by the singularities of $\hat{v}(y; x, \omega)$ above L_1 . Simultaneously the contour F in the α -plane has to be deflected around constant ω_r trajectories of $\alpha_j(\omega)$ which cross the real α -axis as $\omega_i \rightarrow 0$. The trajectory of the TS mode displays this behaviour, therefore F is deflected to F_1 , as shown in Figure 3b. The branch-cuts in the α -plane do not interfere with this process, because as was shown in Appendix A, the upper hyperbola branch-cut does not cross the real α -axis as long as $\omega_i > 0$, the lower hyperbola branch-cut is below the real α -axis for all ω , and the imaginary axis branch-cuts do not depend on ω at all.

Finally, the Briggs method requires one to check the possibility of the coalescing of constant ω_r trajectories originating at opposite sides of the real α -axis. Such an occurrence would be sufficient for the existence of a branch-cut of \hat{v} in the ω -plane, which corresponds to an absolute instability. Investigation of this possibility requires knowledge of all the trajectories $\alpha_j(\omega)$. As discussed in Section 4.1 above, from spatial stability calculations it is only known that for $\omega_i = 0$ all of the higher modes are above the real α -axis. The possibility that their trajectories move into the lower half plane as ω_i is decreased from its value on L , and coalesce among themselves or with the trajectory of the TS mode, cannot be excluded a priori, without performing extensive numerical calculations. This is left for future work, and at the present we make the assumption that coalescing of poles does not occur. The fact that absolute instabilities in boundary layer flow were never observed experimentally supports this assumption hueristically (it was not shown by the Briggs method that an absolute instability is *sufficient* for coalescing of trajectories).

This assumption leads to the conclusion that \hat{v} has no singularities above the real ω -axis, and L can then be deflected to L_1 with the proper deflection of the contour around the poles $\pm\omega_0$.

4.4. Inversion from α to x

First the inversion from α to x is performed according to

$$\hat{v}(y; x, \omega) = \frac{1}{2\pi} \int_{F_1} \Phi(y; \alpha, \omega) e^{i\alpha x} d\alpha \quad (35)$$

To evaluate the integral we construct closed contours in the α -plane and apply the residue theorem. Two different contours are used, one for the domain $x > 0$, downstream of the ribbon, and the other for $x < 0$, upstream, as shown in Figure 3b.

For $x > 0$ the contour is closed in the upper half α -plane with the semicircle Γ_1 of radius r , deflected around the two branch-cuts. The closed contour consists of the section of

F_1 from $-r$ to $+r$, of the sections of the semicircle Γ_1 , and of the four sides of the branch-cuts, marked with the Roman letters I to IV (Figure 3b).

The residue theorem yields

$$\int_{-r}^{+r} + \int_{\Gamma_1} + \int_I + \int_{II} + \int_{III} + \int_{IV} = 2\pi i \sum_{j=1}^{N^{(u)}} \text{Res}[\Phi(y; \alpha, \omega) e^{i\alpha x}]_{\alpha=\alpha_j^{(u)}(\omega)} \quad (36)$$

where the integrand has been omitted, and $N^{(u)}$ is the number of poles above F_1 . The first integral represents integration along the section of F_1 from $-r$ to $+r$. The rest of the integrals represent integration on the sides of the branch-cuts, and the the right hand side is the sum over the residues at the $N^{(u)}$ discrete poles $\alpha_j(\omega)$, designated with the superscript (u).

For the domain $x < 0$ a similar semicircle Γ_2 is constructed in the lower half α -plane, deflected around the branch-cuts there. Similar application of the residue theorem yields

$$\int_{-r}^{+r} + \int_{\Gamma_2} + \int_V + \int_{VI} + \int_{VII} + \int_{VIII} = -2\pi i \sum_{j=1}^{N^{(\ell)}} \text{Res}[\Phi(y; \alpha, \omega) e^{i\alpha x}]_{\alpha=\alpha_j^{(\ell)}(\omega)} \quad (37)$$

The roman letters designate the sides of the branch-cuts as marked in Figure 3b and the residues are calculated at the $N^{(\ell)}$ poles below F_1 , designated with the superscript (ℓ).

As $r \rightarrow \infty$ the first integral in the the left hand side of (36) and (37) approaches the integral in (35). The integral on Γ_1 vanishes for $x > 0$ as $r \rightarrow \infty$, and the integral on Γ_2 vanishes for $x < 0$ as $r \rightarrow \infty$. Assuming all poles are of first order the following result is obtained

$$\hat{v}(y; x, \omega) = \hat{v}_D(y; x, \omega) + \hat{v}_C(y; x, \omega) \quad (38)$$

wherein \hat{v}_D is the discrete spectrum in the ω -plane, given as

$$\hat{v}_D(y; x, \omega) = - \sum_{j=1}^{N^{(u)}} \frac{\omega}{\omega^2 - \omega_0^2} \frac{\Delta(y; \alpha_j^{(u)}(\omega), \omega)}{\frac{\partial \Delta_0(\alpha_j^{(u)}(\omega), \omega)}{\partial \alpha}} e^{i\alpha_j^{(u)}(\omega)x}, \quad x > 0 \quad (39a)$$

$$\hat{v}_D(y; x, \omega) = \sum_{j=1}^{N^{(\ell)}} \frac{\omega}{\omega^2 - \omega_0^2} \frac{\Delta(y; \alpha_j^{(\ell)}(\omega), \omega)}{\frac{\partial \Delta_0(\alpha_j^{(\ell)}(\omega), \omega)}{\partial \alpha}} e^{i\alpha_j^{(\ell)}(\omega)x}, \quad x < 0 \quad (39b)$$

and \hat{v}_C are the continuous spectra

$$\hat{v}_C(y; x, \omega) = \hat{v}_{C_1}(y; x, \omega) + \hat{v}_{C_2}(y; x, \omega) \quad (40)$$

where subscript 1 designates spectra originating from integration around the imaginary axis branch-cut, and 2 designates the spectra originating from the hyperbola branch-cuts as follows:

$$\hat{v}_{C_1}(y; x, \omega) = -\frac{1}{2\pi} \int_I \Phi(y; \alpha, \omega) e^{i\alpha x} d\alpha - \frac{1}{2\pi} \int_{II} \Phi(y; \alpha, \omega) e^{i\alpha x} d\alpha, \quad x > 0 \quad (41a)$$

$$\hat{v}_{C_2}(y; x, \omega) = -\frac{1}{2\pi} \int_{III} \Phi(y; \alpha, \omega) e^{i\alpha x} d\alpha - \frac{1}{2\pi} \int_{IV} \Phi(y; \alpha, \omega) e^{i\alpha x} d\alpha, \quad x > 0 \quad (41b)$$

$$\hat{v}_{C_1}(y; x, \omega) = -\frac{1}{2\pi} \int_V \Phi(y; \alpha, \omega) e^{i\alpha x} d\alpha - \frac{1}{2\pi} \int_{VI} \Phi(y; \alpha, \omega) e^{i\alpha x} d\alpha, \quad x < 0 \quad (42a)$$

$$\hat{v}_{C_2}(y; x, \omega) = -\frac{1}{2\pi} \int_{VII} \Phi(y; \alpha, \omega) e^{i\alpha x} d\alpha - \frac{1}{2\pi} \int_{VIII} \Phi(y; \alpha, \omega) e^{i\alpha x} d\alpha, \quad x < 0 \quad (42b)$$

4.5. Inversion from ω to t

Next \hat{v} is inverted from ω to t according to

$$v(y; x, t) = \int_{L_1} \hat{v}(y; x, \omega) e^{-i\omega t} d\omega \quad (43)$$

The integral vanishes on the straight section of L_1 for $t \rightarrow \infty$, leaving v to be calculated by integrating around the circles surrounding the poles $\pm\omega_0$. Using the residue theorem,

$$v(y; x, t) = \sum \text{Res}[\hat{v}(y; x, \omega) e^{-i\omega t}]_{\omega=\pm\omega_0} \quad (44)$$

Detailed evaluation of (44) is given in Ashpis & Reshotko (1986) and is outlined in the following.

By observing (39) , (41) and (42) , it is seen that \hat{v} consists of sums and integrals of functions of the form

$$G = \frac{\omega}{\omega^2 - \omega_0^2} g(y; x, \omega) \quad (45)$$

It is found that

$$\text{Res}[G]_{\omega=\pm\omega_0} = \pm \frac{1}{2} g(y; x, \pm\omega_0) \quad (46)$$

Using the symmetry property of g ,

$$g(y; x, \omega_0) = \bar{g}(y; x, -\omega_0) \quad (47)$$

where the overbar represents the complex conjugate, it is obtained that

$$\sum \text{Res}[G]_{\omega=\pm\omega_0} = \text{Real}[g(y; x, \omega_0)] \quad (48)$$

Applying these results in (44) leads to the final result for the time-asymptotic form of v as follows

$$v(y; x, t) = v_D(y; x, t) + v_C(y; x, t) \quad (49a)$$

$$v_C(y; x, t) = v_{C_1}(y; x, t) + v_{C_2}(y; x, t) \quad (49b)$$

where the various terms are detailed in the following. The added superscripts (u) and (ℓ) designate the downstream ($x > 0$) and the upstream ($x < 0$) regions, respectively.

The discrete part of v , designated v_D , is:

$$v_D^{(u)}(y; x, t) \sim - \sum_{j=1}^{N^{(u)}} \text{Im} \left\{ \frac{\Delta(y; \alpha_j^{(u)}(\omega_0), \omega_0)}{\frac{\partial \Delta_0(\alpha_j^{(u)}(\omega_0), \omega_0)}{\partial \alpha}} e^{i[\alpha_j^{(u)}(\omega_0)x - \omega_0 t]} \right\}, \quad x > 0 \quad (50a)$$

$$v_D^{(\ell)}(y; x, t) \sim \sum_{j=1}^{N^{(\ell)}} \text{Im} \left\{ \frac{\Delta(y; \alpha_j^{(\ell)}(\omega_0), \omega_0)}{\frac{\partial \Delta_0(\alpha_j^{(\ell)}(\omega_0), \omega_0)}{\partial \alpha}} e^{i[\alpha_j^{(\ell)}(\omega_0)x - \omega_0 t]} \right\}, \quad x < 0 \quad (50b)$$

where the "∼" sign designates that this is the time-asymptotic limit. A non-zero value for (50b) is contingent on existence of poles in the left half-plane as discussed before.

The continuous part of v originating from the imaginary-axis branch-cut, designated v_{C_1} , is:

$$v_{C_1}^{(u)}(y; x, t) \sim -\frac{1}{2\pi} \operatorname{Im} \left\{ \left[\int_0^\infty A_1^{(u)}(y; \sigma, \omega_0) e^{-\sigma x} d\sigma \right] e^{-i\omega_0 t} \right\}, \quad x > 0 \quad (51a)$$

$$v_{C_1}^{(\ell)}(y; x, t) \sim \frac{1}{2\pi} \operatorname{Im} \left\{ \left[\int_0^\infty A_1^{(\ell)}(y; \sigma, \omega_0) e^{+\sigma x} d\sigma \right] e^{-i\omega_0 t} \right\}, \quad x < 0 \quad (51b)$$

where

$$A_1^{(u)}(y; \sigma, \omega_0) = \frac{\Delta(y; i\sigma^+, \omega_0)}{\Delta_0(i\sigma^+, \omega_0)} - \frac{\Delta(y; i\sigma^-, \omega_0)}{\Delta_0(i\sigma^-, \omega_0)} \quad (52a)$$

$$A_1^{(\ell)}(y; \sigma, \omega_0) = \frac{\Delta(y; -i\sigma^+, \omega_0)}{\Delta_0(-i\sigma^+, \omega_0)} - \frac{\Delta(y; -i\sigma^-, \omega_0)}{\Delta_0(-i\sigma^-, \omega_0)} \quad (52b)$$

wherein

$$i\sigma^\pm = \lim_{\epsilon \rightarrow 0^\pm} (\epsilon + i\sigma)$$

The \pm signs correspond to the sides of the imaginary axis branch-cuts, as shown in Figure 3b.

The continuous part of v originating from the hyperbola branch-cuts, designated v_{C_2} , is:

$$v_{C_2}^{(u)}(y; x, t) \sim \frac{1}{2\pi} \operatorname{Real} \left\{ e^{-\sigma_1(\omega_0)x} \int_0^\infty A_2^{(u)}(y; \sigma, \omega_0) e^{-\sigma x} e^{i[\delta_1(\sigma, \omega_0)x - \omega_0 t]} d\sigma \right\}, \quad x > 0 \quad (53a)$$

$$v_{C_2}^{(\ell)}(y; x, t) \sim \frac{1}{2\pi} \operatorname{Real} \left\{ e^{+\sigma_2(\omega_0)x} \int_0^\infty A_2^{(\ell)}(y; \sigma, \omega_0) e^{+\sigma x} e^{i[\delta_2(\sigma, \omega_0)x - \omega_0 t]} d\sigma \right\}, \quad x < 0 \quad (53b)$$

where

$$A_2^{(u)}(y; \sigma, \omega_0) = \left[\frac{\partial \delta_1(\sigma, \omega_0)}{\partial \sigma} + i \right] \cdot \left[\frac{\Delta(y; \alpha_{B_1}^+(\sigma, \omega_0), \omega_0)}{\Delta_0(\alpha_{B_1}^+(\sigma, \omega_0), \omega_0)} - \frac{\Delta(y; \alpha_{B_1}^-(\sigma, \omega_0), \omega_0)}{\Delta_0(\alpha_{B_1}^-(\sigma, \omega_0), \omega_0)} \right] \quad (54a)$$

$$A_2^{(\ell)}(y; \sigma, \omega_0) = \left[\frac{\partial \delta_2(\sigma, \omega_0)}{\partial \sigma} - i \right] \cdot \left[\frac{\Delta(y; \alpha_{B_2}^-(\sigma, \omega_0), \omega_0)}{\Delta_0(\alpha_{B_2}^-(\sigma, \omega_0), \omega_0)} - \frac{\Delta(y; \alpha_{B_2}^+(\sigma, \omega_0), \omega_0)}{\Delta_0(\alpha_{B_2}^+(\sigma, \omega_0), \omega_0)} \right] \quad (54b)$$

σ is an integration variable, subscript B_1 designates the upper hyperbola branch-cut, B_2 the lower one, the superscripts \pm designate the side of the respective branch-cut, as marked in Figure 3b.

$\delta_{1,2}$ and $\sigma_{1,2}$ are the coordinates of the branch-points $\alpha_{BP_{1,2}} = (\delta_{1,2} + i\sigma_{1,2})$ for $\omega = \omega_0$, and are given by the following equations

$$\sigma_{1,2}(\omega_0) = \frac{R}{2} \left\{ \mp 1 + \left[\frac{1}{2} \left(1 + \sqrt{1 + \left(\frac{4\omega_0}{R} \right)^2} \right) \right]^{1/2} \right\} \quad (55)$$

$$\delta_{1,2}(\omega_0) = \frac{\omega_0}{1 \pm 2 \frac{\sigma_{1,2}(\omega_0)}{R}} \quad (56)$$

For $\frac{\omega_0}{R} \ll 1$ it is obtained that

$$\sigma_1(\omega_0) \approx \frac{\omega_0^2}{R} \quad (57a)$$

$$\sigma_2(\omega_0) \approx \frac{\omega_0^2}{R} + R \quad (57b)$$

$$\delta_1(\omega_0) \approx \omega_0 \quad (57c)$$

$$\delta_2(\omega_0) \approx -\omega_0 \quad (57d)$$

5. Description of the results

The expressions (50) to (56) show that the vibrating ribbon excites discrete and continuous spectra, whose frequency in the time-asymptotic limit is equal to the frequency of the ribbon.

The discrete spectrum consists of the spatial eigenmodes of the flow. These are discrete travelling waves with frequency ω_0 and wavenumber $\alpha_{j_r}(\omega_0)$. The phase velocity of the wave is

$$c_j = \frac{\omega_0}{\alpha_{j_r}(\omega_0)} \quad (58)$$

The growth factor is $e^{-\alpha_{j_i}(\omega_0)x}$, and the coupling coefficient, indicating the extent to which the mode is excited, is

$$K_j = \frac{\Delta(y; \alpha_j(\omega_0), \omega_0)}{\frac{\partial \Delta(\alpha_j(\omega_0), \omega_0)}{\partial \alpha}} \quad (59)$$

The quadrant in which the pole is located then determines the properties of its corresponding wave. Its region of influence is determined by its position above or below the contour F_1 . The various possibilities are depicted in Figure 4. Poles in the right half α -plane correspond to waves propagating in the positive x direction (positive phase velocity), and the ones in the left half α -plane correspond to waves travelling in the negative x direction. Growth in the region $x > 0$, downstream of the ribbon, is if the corresponding pole is below the real α -axis; and in the upstream region, $x < 0$, growth in the negative x direction is if the pole is above the real α -axis. The right half α -plane was thoroughly investigated numerically by various researchers (see discussion in Section 4 above), and the cases described in Figure 4 (a-ii) and (d-i) were never found. The cases (b-ii) and (c-ii) cannot be expected to be found when extending these computations to the left half α -plane.

For $x \rightarrow \infty$, the higher modes decay spatially, leaving the Tollmien-Schlichting mode to be the dominant mode in the downstream region, and the summation in (50a) can be omitted.

The continuous spectra affect the regions upstream and downstream of the ribbon. In each region it consists of two parts; the one described by (51), consisting of a superposition of standing waves, and the one given by (53) is a superposition of travelling waves. In both cases the waves decay away from the ribbon as $x \rightarrow \pm\infty$, although growth is possible for finite x close to the origin.

6. Discussion

In the work presented here we have revisited the vibrating ribbon problem which was first done by Gaster (1965). For the purpose of comparing the two works, we use the notation G when referring to Gaster's work, and present its outline in Appendix C. We have written the equations and the boundary conditions in terms of the disturbance normal velocity, while G used the disturbance stream function. As shown in Appendix C, the two formulations are equivalent and lead to the same equation and boundary conditions. Except for this minor difference, we followed the formulation of G up to the point where the double transform is applied (Equation (9)). From there on our solution method differs considerably. We expressed the solution in terms of the fundamental solutions of the Orr-Sommerfeld equation, exercised some care in the evaluation procedure, and applied the Briggs method to obtain the time-asymptotic solution. In G the solution is written in terms of a nonspecified complete solution of the the Orr-Sommerfeld equation and boundary conditions, and the inversion contour is not determined in a straightforward way (see Appendix C for details).

A significant outcome achieved by the present work is that the solution includes the continuous spectra, which are missing from G . The wave components of these spectra are identical to the spatial continuous spectra obtained in Grosch and Salwen (1978) and Salwen and Grosch (1981) by looking for pure oscillatory eigenmodes of the the Orr-Sommerfeld equation. Here these eigenmodes emerge in a natural way, simply by constructing branch-cuts in the complex planes, as required whenever a complex square-root function is encountered.

The discrete spectrum obtained in the present work is equivalent to the one in G , with the exception of the factor of $1/2$ which appears there (compare (C11) to (50a)). In addition, the result in G depends on assumptions involving the sign of the group velocity (see Appendix C). No such assumptions are used in the present analysis. The reason for the discrepancy by the factor of $1/2$ is an error in the computation of the residue at

$\omega = \omega_0$: The inversion contour in G was taken along the real ω -axis (Figure 9). In that case the following expression, appearing in (C6) takes the form

$$\lim_{\omega_i \rightarrow 0} \frac{\omega}{\omega^2 - \omega_0^2} = \frac{\omega_r}{\omega_r^2 - \omega_0^2} - i\frac{\pi}{2}[\delta(\omega_r + \omega_0) + \delta(\omega_r - \omega_0)] \quad (60)$$

The contribution from the term containing the δ functions, which is equal to the contribution from term preceding it, was not taken into account in G .

It was obtained here that the ribbon has a downstream influence by excitation of both the discrete and continuous spectra. The new finding is that it also has an upstream influence via the continuous spectra. It was shown that the possibility of an additional upstream influence by excitation of the discrete spectra needs also to be considered. This can be verified or excluded only by numerical search for poles in the left half plane, which correspond to spatial eigenvalues with negative real parts for positive frequencies. The spatial decay in the time-asymptotic limit of the continuous spectra is much greater in the upstream direction compared to the downstream direction. This is concluded from (57), showing that at large Reynolds numbers $\sigma_2 \gg \sigma_1$, which affects the exponential decay terms preceding the integrals in (53).

The distinction between singularities affecting the upstream region and the ones affecting the downstream region is useful also in clarifying the difficulty expressed in Salwen and Grosch (1981). They point out that the wave component of the continuous spectra which propagates upstream from $x = \infty$ and the standing waves whose amplitudes increase towards $x = \infty$ are not physically acceptable. This difficulty is resolved by the analysis here, which shows that these waves are excited only in the upstream region of the ribbon and therefore *are* physically acceptable.

Once solved systematically and correctly, the complex plane contains all the discrete and continuous singularities, and the the solution can serve as proof of completeness of the eigenfunction expansion in the spatial case. This is in analogy with the proof of completeness for the temporal case done by Salwen & Grosch (1981) by comparing to the solution of Gustavsson (1979). Although proof of completeness for this case is reported in

an abstract by Salwen, Kelly and Grosch (1980), details were never published and could not be obtained from the authors.

Our solution also sheds light on the difficulties in the IBVP solutions reviewed in Section 1. In these solutions a Laplace transform was applied to the longitudinal spatial coordinate x , which is equivalent to the Fourier transform of a function causal in x (A 90 degree rotation relates the Laplace S -plane to the Fourier α -plane). Therefore, formally, the application of the Laplace transform should yield the same discrete and continuous singularities as the Fourier transform. However, the complex S -planes in the work of Tsuge & Rogler (1983) and of Aldoss (1982) do not include the counterparts of the imaginary axis branch-cuts. In addition there is an inconsistency in these works, as well as in Tumin & Fedorov (1984), where branch-cut singularities protrude into what should be a half plane of analyticity of the S -plane. As is shown, the disturbance introduced by the vibrating ribbon has an upstream influence, at least through the continuous spectra, and so will any disturbance introduced at $x = 0$. By applying the Laplace transform this possibility is excluded, and it is suggested that this is the source of the mathematical inconsistency, and that it is incorrect to use the Laplace transform in these problems.

Appendix A. The functions μ and ζ and evaluation of r_j

The essentials of the evaluation of the functions μ and ζ and the four solutions r_j of the characteristic equation (15) are contained in this Appendix. The detailed evaluation can be found in Ashpis & Reshotko (1986).

A.1 The complex square root function

r_j are evaluated as the complex square roots given in Section 3.1 as

$$r_{3,1} = \pm(\mu^2)^{1/2} \quad (16)$$

$$r_{4,2} = \pm(\alpha^2)^{1/2} \quad (17)$$

We follow in detail the well known elementary steps to evaluate the square roots. To exercise this extra care we first review the complex square root function $F = Z^{1/2}$. F has two single valued branches F^+ and F^- , which are related by $F^+ = -F^-$. To make F single valued, it is needed (i) to construct a branch-cut in the Z -plane, (ii) to characterize F^+ and F^- by a specified definition, and (iii) to select one of the branches F^+ or F^- to represent F .

These three steps are executed as follows: (i) Any line from the branch-point $Z = 0$ to ∞ is an acceptable branch-cut, and we select the negative real Z -axis as the branch-cut. (ii) We define F^+ to be the branch of F that yields real positive F at real positive Z , F^- is then the branch that yields real negative F at real positive Z . (iii) Finally, we choose the single valued function to be represented by the branch F^+ . This process establishes a convention for defining the single-valued complex square-root function which is used throughout this paper.

This convention ensures that

$$\text{Real}(F) > 0 \text{ for all } Z \quad (A1)$$

The situation is illustrated in Figure 5 . It is easy to demonstrate that (A1) will not be valid for any other selection of a branch-cut in the Z -plane.

A.2 evaluation of r_1 and r_3

Let Z be defined as

$$Z = \alpha^2 + iR(\alpha - \omega) \quad (A2)$$

then, from (11)

$$\mu = Z^{1/2} \quad (A3)$$

where μ is a single-valued function, according to the convention described above. Following (16) it is obtained that

$$r_1 = -\mu \quad (A4)$$

$$r_3 = \mu \quad (A5)$$

Z depends on α , ω and R . For fixed R , either ω , or α , can be taken as a parameter.

A.2.1 μ with ω as parameter

The case where ω is the parameter is discussed first. In this case μ can be viewed as a mapping from the α -plane to the μ -plane via the auxiliary plane Z . The various planes are illustrated in Figure 6.

The mapping from the α -plane to the Z -plane is investigated in the following.

Let

$$Z = Z_r + iZ_i \quad (A6)$$

$$\alpha = \alpha_r + i\alpha_i \quad (A7)$$

$$\omega = \omega_r + i\omega_i \quad (A8)$$

Substitution into (A2) and equating the real and imaginary parts yields

$$\left(\alpha_i + \frac{R}{2}\right) = \frac{Z_i + R\omega_r}{2\alpha_r} \quad (A9a)$$

$$\left(\alpha_i + \frac{R}{2}\right)^2 - \alpha_r^2 = \frac{R^2}{4} + R\omega_i - Z_r \quad (A9b)$$

which shows that constant Z_r and Z_i lines are mapped into hyperbolas in the α -plane. (A9a) represents a family of canonical hyperbolas of the first kind, and (A9b) represents a family of canonical hyperbolas of the second kind, both shifted to $\alpha_i = -R/2$. In addition to the R -dependence, (A9a) depends only on ω_r , the real part of ω . (A9b) depends only on its imaginary part ω_i . The mapping is illustrated in Figure 6 for the case of a pure real and positive ω . The real Z -axis is mapped to the hyperbolas a_1 and a_2 ; the imaginary Z -axis is mapped to the hyperbolas b_1 and b_2 . The quadrants of the Z -plane and the domains in the α -plane into which they are mapped are marked with the roman letters I to IV . The branch-point $Z = 0$ is mapped to the points BP_1 and BP_2 . These points are the intersection points of the hyperbolas a_1 with b_1 , and of a_2 with b_2 . It then follows that the branch-cut in the Z -plane is mapped into the two marked sections of the hyperbolas a_1 and a_2 , from the branch-points $BP_{1,2}$ to $\pm\infty$.

The coordinates of the branch-points and equations of the branch-cuts are given in Ashpis & Reshotko (1986). The branch-points vary with ω as follows: As ω_i increases the branch-points move towards $\pm i\infty$ along the hyperbolas a_1 and a_2 , respectively. The upper branch-point BP_1 is above the real α -axis for $\omega_i > 0$. As ω_i decreases to negative values BP_1 moves below the real α -axis. The lower branch-point BP_2 stays below the real α -axis for all ω_i . For $\omega_r < 0$ the picture is symmetric with respect to the imaginary α -axis.

It follows from the previous discussion that the auxiliary Z -plane, with the branch-cut along the negative real axis is mapped into the right half μ -plane. Since the whole the α -plane is mapped to the Z -plane, it follows that with the specified branch-cuts it is

ensured that

$$\text{Real}(\mu) > 0 \text{ for all } \alpha \text{ and } \omega. \quad (\text{A10})$$

A practical formula for calculation of μ is given by

$$\mu = \sqrt{\frac{r}{2}} \left[\sqrt{1 + \frac{Z_r}{r}} \pm i \sqrt{1 - \frac{Z_r}{r}} \right] \quad (\text{A11})$$

where

$$Z_r = \alpha_r^2 - \alpha_i^2 - R(\alpha_i - \omega_i) \quad (\text{A12})$$

$$Z_i = 2\alpha_i\alpha_r + R(\alpha_r - \omega_r) \quad (\text{A13})$$

$$r = (Z_r^2 + Z_i^2)^{1/2} \quad (\text{A14})$$

The + sign is used in regions I and II, the – sign in III and IV of the α -plane (Figure 6).

A.2.2 μ with α as parameter

When α is taken as the parameter in (A2) with fixed R , μ can be viewed as a mapping from the ω -plane to the μ -plane via the auxiliary plane Z , as depicted in Figure 7. We obtain in a similar fashion

$$\omega_i = \frac{1}{R}(Z_r - \alpha_r^2 + \alpha_i^2 + R\alpha_i) \quad (\text{A15})$$

$$\omega_r = \frac{1}{R}(-Z_i + 2\alpha_i\alpha_r + R\alpha_r) \quad (\text{A16})$$

These expressions show that constant Z_r and Z_i lines in the Z -plane are mapped into straight lines in the ω -plane.

The branch-point $Z = 0$ is mapped into the point BP_0 whose coordinates are

$$\omega_{BP_0} = \eta_0 + i\sigma_0 \quad (A17)$$

where

$$\sigma_0 = -\frac{1}{R}[\alpha_r^2 - (\alpha_i^2 + R\alpha_i)] \quad (A18)$$

$$\eta_0 = \alpha_r \left(1 + \frac{2\alpha_i}{R}\right) \quad (A19)$$

The branch-cut extends from BP_0 to $-\infty$ in the lower half ω -plane parallel to the imaginary axis. For $\alpha_i = 0$ the branch point forms the trajectory $\sigma_0 = -\frac{1}{R}\eta_0^2$, therefore the branch-cut is always below the real ω -axis.

This branch-cut is mapped into the branch-cut in the Z -plane therefore it follows that

$$\text{Real}(\mu) > 0 \text{ for all } \omega \text{ and } \alpha. \quad (A20)$$

A.3 Evaluation of $r_{2,4}$ and the function ζ

A similar analysis is applied to (17) and (21). As noted in Section 3.1, it is useful to avoid ambiguity by defining the function ζ as

$$\zeta^2 = (\alpha - i\varepsilon)(\alpha + i\varepsilon) \quad (A21)$$

(For a similar idea see Carrier *et al* (1966) pg 315, 346).

Then

$$\alpha^2 = \lim_{\varepsilon \rightarrow 0} \zeta^2 \quad (A22)$$

We define z as

$$z = (\alpha - i\varepsilon)(\alpha + i\varepsilon) \quad (A23)$$

and it follows that

$$\zeta = z^{1/2} \quad (A24)$$

where ζ is a single valued function subject to the previous convention regarding the complex square-root. Therefore

$$r_2 = -\lim_{\varepsilon \rightarrow 0} \zeta \quad (\text{A25})$$

$$r_4 = \lim_{\varepsilon \rightarrow 0} \zeta \quad (\text{A26})$$

Similar to the treatment of μ , we view ζ as a mapping of the α -plane, via the auxiliary plane z (Figure 8). The process here is, however, simpler because ζ does not depend on R or ω .

As before, we select a branch-cut in the z -plane along the negative real axis, therefore the whole z -plane is mapped into the right half ζ -plane.

The mapping from the α -plane to the z -plane is given by

$$\alpha_i^2 - \alpha_r^2 = \varepsilon^2 - z_r \quad (\text{A27a})$$

$$\alpha_i = \frac{z_i/2}{\alpha_r} \quad (\text{A27b})$$

where

$$z = z_r + iz_i \quad (\text{A28})$$

(A27a) shows that constant z_r lines in the z -plane are mapped into a family of canonical hyperbolas of the second kind in the α -plane. (A27b) shows that constant z_i lines are mapped into a family of canonical hyperbolas of the first kind. The branch-point $z = 0$ is mapped to the points $\pm i\varepsilon$ in the α -plane, and the branch-cut is mapped to the sections of the imaginary α -axis, from the branch-points to $\pm\infty$, as shown in Figure 8. Selecting these sections as branch-cuts ensures that

$$\text{Real}(\zeta) > 0 \text{ for all } \alpha \quad (\text{A29})$$

A working formula for the calculation of ζ is given as

$$\zeta = \sqrt{\frac{a}{2}} \left[\sqrt{1 + \frac{z_r}{a}} \pm i \sqrt{1 - \frac{z_r}{a}} \right] \quad (\text{A30})$$

where

$$z_r = \alpha_r^2 - \alpha_i^2 + \varepsilon^2 \quad (A31)$$

$$z_i = 2\alpha_r\alpha_i \quad (A32)$$

$$a = (z_r^2 + z_i^2)^{1/2} \quad (A33)$$

and the $+$ is taken in the quadrants (1) and (3), and the $-$ in quadrants (2) and (4) of the α -plane, as marked in Figure 8.

As $\varepsilon \rightarrow 0$ the two branch-points approach the origin $\alpha = 0$. This point, however remains a regular point of ζ . Therefore in the limit $\varepsilon \rightarrow 0$ the branch-cuts coincide with the whole imaginary α -axis, with the exclusion of the point of origin.

Also as $\varepsilon \rightarrow 0$ (20) can be written as

$$\zeta = \text{sign}(\alpha_r) \cdot \alpha \quad (A34)$$

Appendix B. Symmetry properties

The function Φ exhibits the following symmetry properties

$$\Phi(y; \alpha, \omega) = \overline{\Phi}(y; -\overline{\alpha}, -\overline{\omega}) \quad (B1)$$

where the overbar designates the complex conjugate. This property follows from the Orr-Sommerfeld equation and also from the properties of the double Fourier transform of a real function.

The single Fourier transform of the real function v has the property

$$\hat{v}(y; x, \omega) = \overline{\hat{v}}(y; x, -\overline{\omega}) \quad (B2)$$

It follows that

$$\Delta_0(\alpha, \omega) = \overline{\Delta_0}(-\overline{\alpha}, -\overline{\omega}) \quad (B3)$$

and that

$$\alpha_j(\omega) = -\overline{\alpha}_j(-\overline{\omega}) \quad (B4)$$

$$\omega_j(\alpha) = -\overline{\omega}_j(-\overline{\alpha}) \quad (B5)$$

Additional details related to these properties are given in Ashpis & Reshotko (1986). It is demonstrated there that the symmetry properties are not valid with a choice of branch-cuts other than those specified in Appendix A.

Appendix C. Outline of Gaster's solution (1965)

Gaster's formulation and solution of the vibrating ribbon problem (Gaster (1965)) is summarized in this appendix. For brevity we here refer to Gaster (1965) as G.

We found some details in G somewhat difficult to follow, mainly due to the lack of accompanying figures describing the complex planes. It was also noted in private communication (Gaster, 1984) that G contains some printing errors and has an omission of a short paragraph. For the purpose of comparison between G and the present work, we find it useful to outline the solution of G in this Appendix and to provide a supplementary figure.

Let us designate the disturbance stream function as $\psi(y; x, t)$ and its double transform as $\Psi(y; \alpha, \omega)$, and use the notations of the present work: Then the disturbance stream function Φ in G is Ψ in our notation; the frequency β in G is ω in our notation; and the frequency of the ribbon ω in G is ω_0 in our notation. The other pertinent notations are identical.

The formulation of the problem in the present work follows the one in G, except that in G the formulation is in terms of the disturbance stream function ψ , while here it is done in terms of the disturbance normal velocity v .

After a double transform, G obtains the Orr-Sommerfeld equation for Ψ

$$(\bar{U}(y) - \omega/\alpha)(\Psi'' - \alpha^2\Psi) - \bar{U}''(y)\Psi = (-i/\alpha R)(\Psi^{IV} - 2\alpha^2\Psi'' + \alpha^4\Psi) \quad (C1)$$

subject to the boundary conditions

at $y = 0$:

$$\Psi(0; \alpha, \omega) = -\frac{1}{\alpha} \frac{\omega}{\omega^2 - \omega_0^2} \quad (C2a)$$

$$\frac{\partial \Psi(0; \alpha, \omega)}{\partial y} = 0 \quad (C2b)$$

as $y \rightarrow \infty$:

$$\Psi, \quad \frac{\partial \Psi}{\partial y} \rightarrow 0 \quad (C3a)$$

since

$$v = -\frac{\partial \Psi}{\partial x} \quad (C3b)$$

then

$$\Phi(y; \alpha, \omega) = -i\alpha \Psi(y; \alpha, \omega) \quad (C4)$$

From (C2a)

$$\alpha = -\frac{\omega}{\omega^2 - \omega_0^2} \frac{1}{\Psi(0; \alpha, \omega)} \quad (C5)$$

which yields after substitution into (C4)

$$\Phi(y; \alpha, \omega) = \frac{i\omega}{\omega^2 - \omega_0^2} \frac{\Psi(y; \alpha, \omega)}{\Psi(0; \alpha, \omega)} \quad (C6)$$

The inversion to the physical domain in G differs from the one performed in the present work in the way the inversion contours are determined, and in the use of the symmetry of Ψ with respect to α and ω .

Two possible inversion contours in the α -plane are considered by G, and the correct contour is selected based on results of the next inversion from ω to t . The inversion from α to x is essentially similar to the one done here, although G uses the symmetry property of Ψ with respect to real α and ω , but the inversion from ω to t is different than the one used here. The closed contour constructed by G for application of the residue theorem is shown in Figure 9. We drew this figure based on the description in G, and provide it here for illustration. It is argued in G that the inversion integral vanishes for $t \rightarrow \infty$ on the section Λ_2 of the contour. This argument utilizes assumptions which involve the sign of the group velocity.

The result for the dominant TS mode obtained in G is

$$v(y; x, t) = -\text{Im} \left\{ \frac{1}{2} \frac{\Psi(y; \alpha(\omega_0), \omega_0)}{\frac{\partial \Psi(0; \alpha(\omega_0), \omega_0)}{\partial \alpha}} e^{i[\alpha(\omega_0) - \omega_0 t]} \right\} \quad (C7)$$

Ψ is a linear combination of the fundamental solutions of the Orr-Sommerfeld equation. The constants, corresponding to the C_j 's of (9) in the present work, were not evaluated in G.

In order to compare the results we write (C7) in terms of the fundamental solutions Φ and Δ (see (9) and (28)), as follows:

Using (C4) for the Ψ -ratio in (C6) yields

$$\frac{\Psi(y; \alpha, \omega)}{\Psi(0; \alpha, \omega)} = \frac{\Phi(y; \alpha, \omega)}{\Phi(0; \alpha, \omega)} \quad (C8)$$

substitution of (27) into (C8) yields

$$\frac{\Psi(y; \alpha, \omega)}{\Psi(0; \alpha, \omega)} = \frac{\Delta(y; \alpha, \omega)}{\Delta_0(\alpha, \omega)} \quad (C9)$$

then (C6) is

$$\Phi(y; \alpha, \omega) = \frac{i\omega}{\omega^2 - \omega_0^2} \frac{\Delta(y; \alpha, \omega)}{\Delta_0(\alpha, \omega)} \quad (C10)$$

and (C7) takes the form

$$v(y; x, t) = -\text{Im} \left\{ \frac{1}{2} \frac{\Delta(y; \alpha(\omega_0), \omega_0)}{\frac{\partial \Delta_0(\alpha(\omega_0), \omega_0)}{\partial \alpha}} e^{i[\alpha(\omega_0) - \omega_0 t]} \right\} \quad (C11)$$

References

- Aldoss, T .K. 1982 Initial value study of effects of distributed roughness on boundary layer transition. Ph.D. Dissertation, Case Western Reserve University.
- Ashpis, D. & Reshotko, E. 1985 The vibrating ribbon problem - revisited. *Bull. Am. Phys. Soc.* **30** (10), 1708.
- Ashpis, D. & Reshotko, E. 1986 On the application of Fourier transforms to the linear stability analysis of Boundary layers. Case Western Reserve University Report FTAS/TR-86-187. Also as: D. E. Ashpis, Ph.D. Dissertation, Case Western Reserve University, 1986.
- Ashpis, D. & Reshotko, E. 1990 The vibrating ribbon problem revisited. *J. Fluid Mech.* **213**, 531-547.
- Bers, A. 1983 Space-time evolution of plasma instabilities - absolute and convective. in: *Basic Plasma Physics I* (A. A. Galeev & R. N. Sudan, eds.), 451-517, North-Holland.
- Briggs, R. J. 1964 *Electron-Stream Interaction with Plasmas*, MIT Press.
- Case, K. M. 1960 Stability of inviscid plane Couette flow, *Phys. Fluids* **3**, 143-158.
- Case, K. M. 1961 Hydrodynamic stability and the inviscid limit. *J. Fluid Mech.* **10**, 420-429.
- Gaster, M. 1965 On the generation of spatially growing waves in a boundary layer. *J. Fluid Mech.* **22**, 433-441.
- Gaster, M. 1984 Private communication.

- Gaster, M. & Jordinson, R. 1975 On the eigenvalues of Orr-Sommerfeld equation .
J. Fluid Mech. **72**, 121-133.
- Grosch, C. E. & Salwen, H. 1978 The continuous spectrum of the Orr-Sommerfeld equation. Part 1. The spectrum and the eigenfunctions. *J. Fluid Mech.* **87**, 33-54.
- Gustavsson, L. H. 1979 Initial-value problem for boundary layer flows. *Phys. Fluids* **22**, 1602-1605.
- Huerre P. 1987 Spatio-temporal instabilities in closed and open flows. in:
The Proceedings of the International Workshop on Instabilities and Non-Equilibrium Structures held in Valparaiso, Chile, December 16-21, 1985 (E. Tirapegui & D. Villanroel, eds.), 141-177, Reidel.
- Huerre P. & Monkewitz, P. A. 1985 Absolute and convective instabilities in free shear layers. *J. Fluid Mech.* **159**, 151-168.
- Hultgren, L. S. & Aggarwal, A. K. 1987 Absolute instability of the Gaussian wake profile. *Phys. Fluids* **30**, 3383-3387.
- Hultgren, L. S. & Gustavsson, L. H. 1981 Algebraic growth of disturbances in a laminar boundary layer, *Phys. Fluids* **24**, 1000-1004.
- Koch, W. 1986 Direct resonances in Orr-Sommerfeld problems. *Acta Mechanica* **58**, 11-29.
- Leib, S. J. & Goldstein, M. E. 1986 The generation of capillary instabilities in a liquid jet. *J. Fluid Mech.* **168**, 479-500.
- Lin, S. P. & Lian Z. W. 1989 Absolute instability of a liquid jet in a gas. *Phys. Fluids A* **1** (3), 490-493.

- Mack, L. M. 1976 A numerical study of the temporal eigenvalue spectrum of the Blasius boundary layer. *J. Fluid Mech.* **73**, 497-520.
- Miklavčič, M. & Williams, M. 1982 Stability of mean flows over an infinite flat plate. *Arch. Rational Mech. Anal.* **80**(1), 57-69.
- Monkewitz, P. A. 1988 The absolute and convective nature of instability in two-dimensional wakes at low Reynolds numbers. *Phys. Fluids* **31**, 999-1006.
- Monkewitz, P. A. & Sohn, K. D. 1986 Absolute instability in hot jets and their control. AIAA Paper No. 86-1882.
- Murdock, J. W. & Stewartson, K. 1977 Spectra of the Orr-Sommerfeld Equation. *Phys. Fluids* **20**, 1404-1411.
- Pierrehumbert, R. T. 1986 Spatially amplifying modes of the Charney baroclinic instability problem. *J. Fluid Mech.* **170**, 293-317.
- Salwen, H., Kelly, K. A. & Grosch, C. E. 1980 Completeness of spatial eigenfunctions for the boundary layer. *Bull. Am. Phys. Soc.* **25** (9), 1085.
- Salwen, H. & Grosch, C. E. 1981 The continuous spectrum of the Orr-Sommerfeld equation. Part 2. Eigenfunction expansions. *J. Fluid Mech.* **104**, 445-465.
- Schubauer, G. B. & Skramstad, H. K. 1947 Laminar boundary layer oscillations and transition on a flat plate. *J. Aeros. Sci.* **14**, 69-76. also: NACA Report 909, 1948.
- Tam, C. K. W. 1971 Directional acoustic radiation from a supersonic jet generated by shear layer instability. *J. Fluid Mech.* **46**, 757-768.
- Tam, C. K. W. 1978 Excitation of instability waves in a two-dimensional shear layer

by sound. *J. Fluid Mech.* **89**, 357-371.

Tsuge, S. & Rogler, H. L. 1983 The two-dimensional, viscous boundary-value problem for fluctuations in boundary layers. AIAA Paper No. 83-0044.

Tumin, A. M. & Fedorov, A. V. 1983 Spatial growth of disturbances in a compressible boundary layer. *PMTF (S.S.S.R.)* **4**, 110-118. translation: *J. App. Mech. Tech. Phys.*, 548-554.

Tumin, A. M. & Fedorov, A. V. 1984 Excitation of instability waves by a localized vibrator in a boundary layer. *PMTF (S.S.S.R.)* **6**, 65-72. translation: NASA TM-77873, 1985.

Yang, X. & Zebib, A. 1989 Absolute and convective instability of a cylinder wake. *Phys. Fluids A* **1**, 689-696.

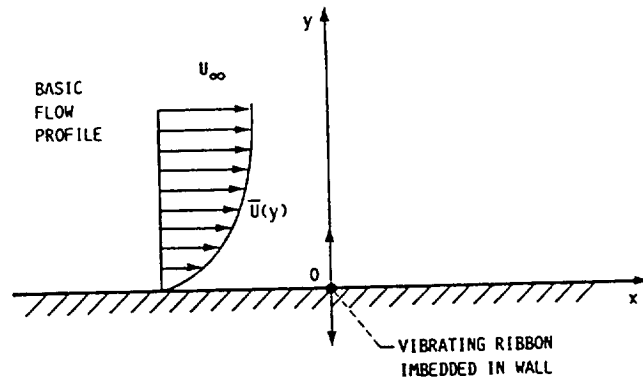


FIGURE 1.

Figure 1. Model of the vibrating ribbon problem.

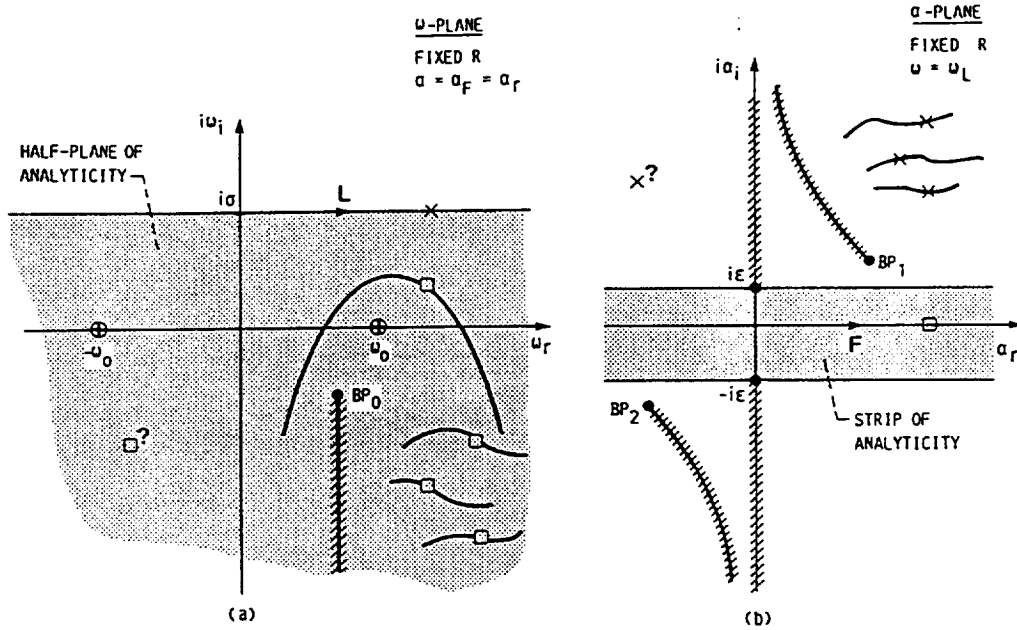


FIGURE 2.

Figure 2. Undeflected contours for the inversion integrals (schematic).

The points marked with \square in (a) indicate poles for the α_r marked with \square in (b). The curves passing through these points are trajectories $\omega_j(\alpha_r)$. Points marked with \times in (b) are poles for ω marked with \times in (a). The curves passing through these points are trajectories $\alpha_j(\omega_L)$. The branch cut in (a) is for $\alpha = \alpha_r$. The branch cuts in (b) are for $\omega = \omega_L$. The question-mark symbols ? in the left half-planes designate yet unknown existence of poles.

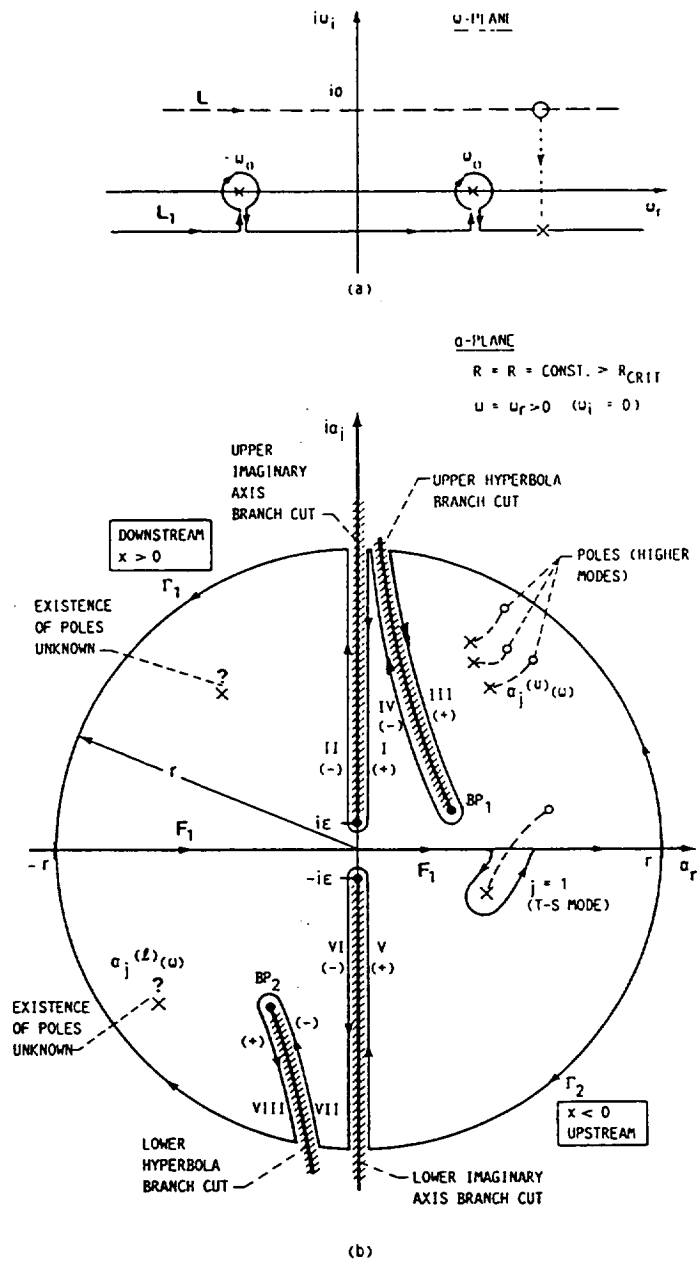


FIGURE 3.

Figure 3. (a) Integration contour in the ω -plane.
 (b) Closed integration contours in the α -plane.

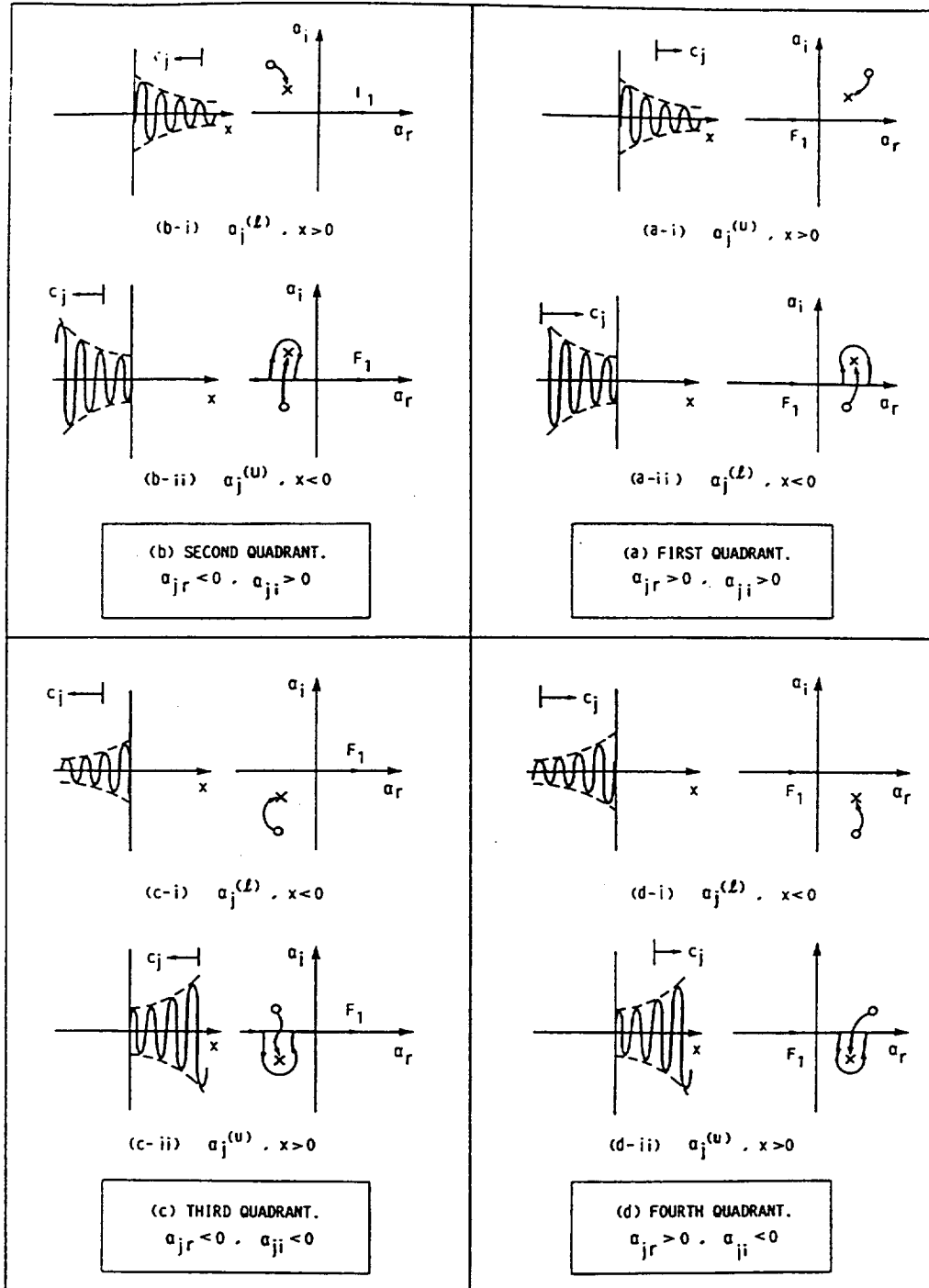


FIGURE 4.

Figure 4. Effects of the location of the pole in the α -plane on its corresponding wave for $\omega_r > 0$.

\times designates the α_j for $\omega_i = 0$, \circ designates α_j for $\omega = \omega_L$.

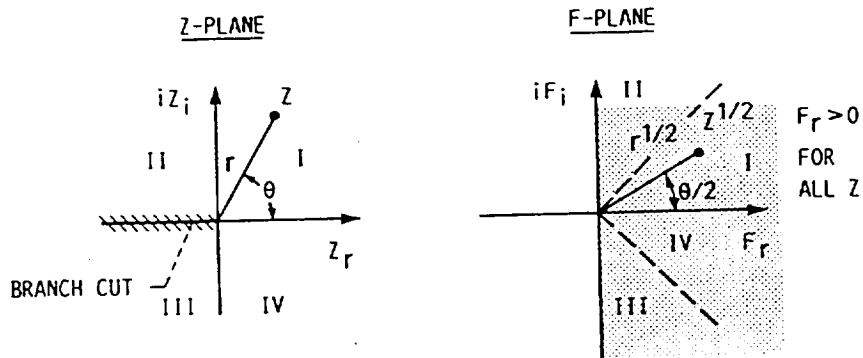


FIGURE 5.

Figure 5. Illustration of the mapping $F = Z^{1/2}$ for the branch F^+ . Roman letters indicate the quadrants in the Z -plane and their image in the F -plane.

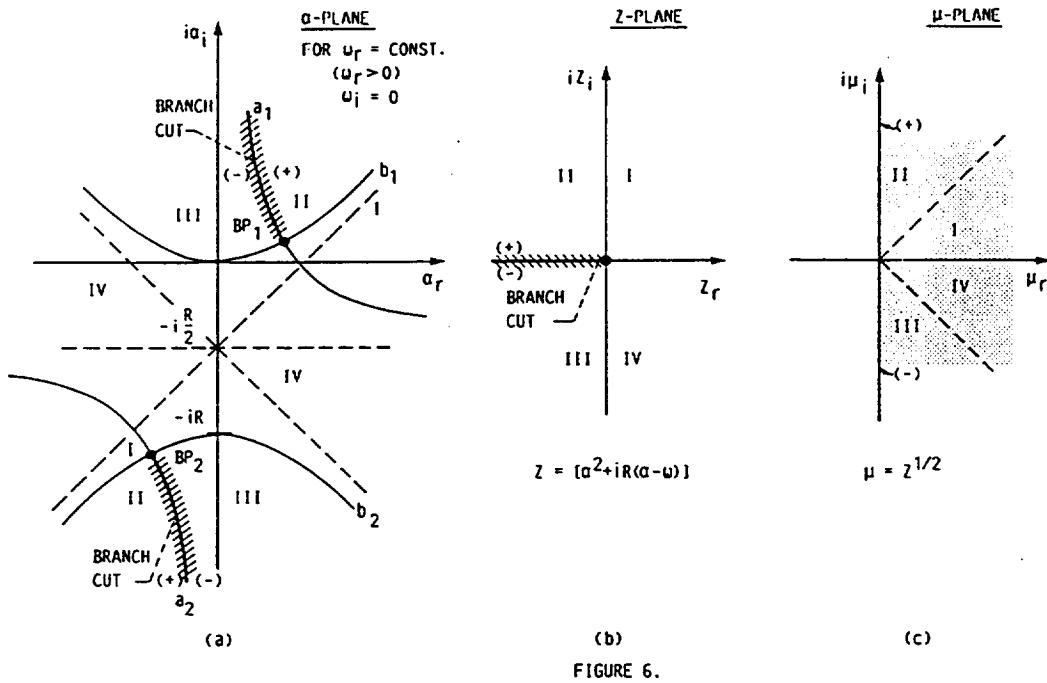


Figure 6. The mapping from the α -plane to the μ -plane via the auxiliary plane Z .

The hyperbolas a_1 and a_2 are mapped into $Z_i = 0$, the hyperbolas b_1 and b_2 are mapped into $Z_r = 0$. the (+) and (-) indicate the two sides of the branch cut. Roman letters indicate the quadrants of the Z -plane and their images in the μ and α planes.

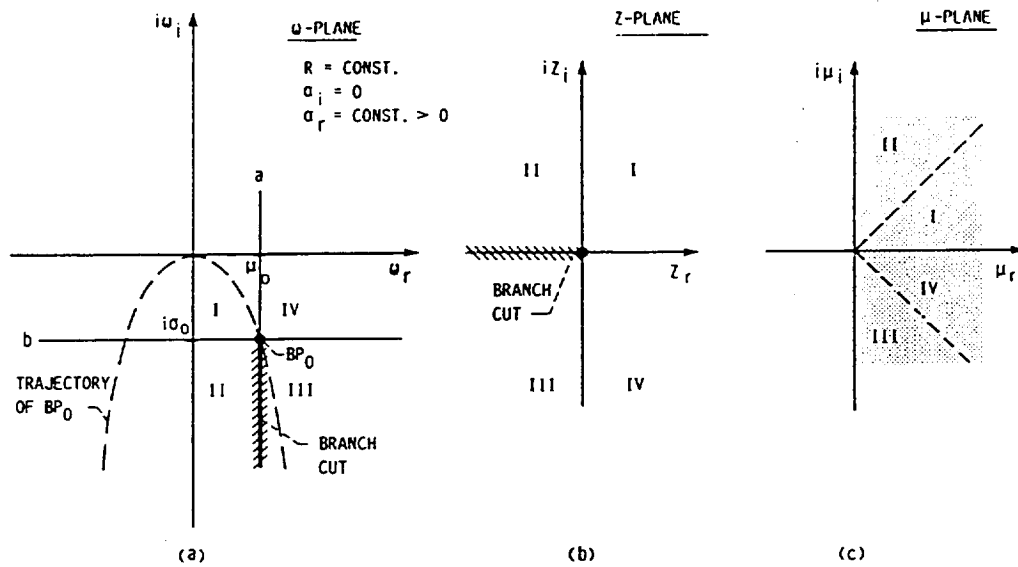


FIGURE 7.

Figure 7. The mapping from the ω -plane to the μ -plane via the auxiliary Z -plane.

The line a is mapped into $Z_i = 0$, and the line b is mapped into $Z_R = 0$.

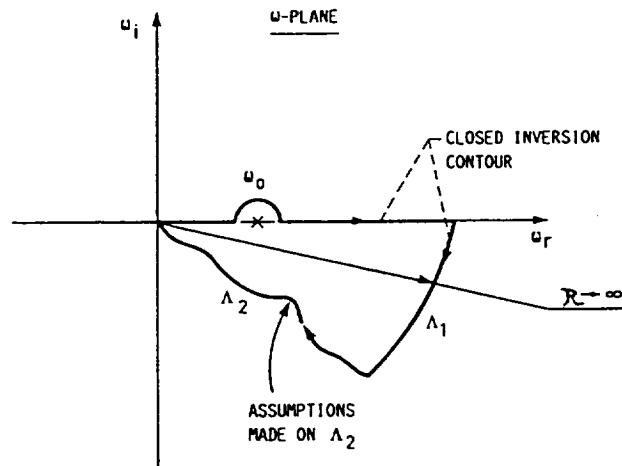


FIGURE 9.

Figure 9. Illustration of Gaster's (1965) inversion contour in the ω -plane.

REPORT DOCUMENTATION PAGE			Form Approved OMB No. 0704-0188	
Public reporting burden for this collection of information is estimated to average 1 hour per response, including the time for reviewing instructions, searching existing data sources, gathering and maintaining the data needed, and completing and reviewing the collection of information. Send comments regarding this burden estimate or any other aspect of this collection of information, including suggestions for reducing this burden, to Washington Headquarters Services, Directorate for Information Operations and Reports, 1215 Jefferson Davis Highway, Suite 1204, Arlington, VA 22202-4302, and to the Office of Management and Budget, Paperwork Reduction Project (0704-0188), Washington, DC 20503.				
1. AGENCY USE ONLY (Leave blank)	2. REPORT DATE July 1998	3. REPORT TYPE AND DATES COVERED Technical Memorandum		
4. TITLE AND SUBTITLE Excitation of Continuous and Discrete Modes in Incompressible Boundary Layers			5. FUNDING NUMBERS WU-522-31-23-00 ZTof	
6. AUTHOR(S) David E. Ashpis and Eli Reshotko				
7. PERFORMING ORGANIZATION NAME(S) AND ADDRESS(ES) National Aeronautics and Space Administration Lewis Research Center Cleveland, Ohio 44135-3191			8. PERFORMING ORGANIZATION REPORT NUMBER E-11271	
9. SPONSORING/MONITORING AGENCY NAME(S) AND ADDRESS(ES) National Aeronautics and Space Administration Washington, DC 20546-0001			10. SPONSORING/MONITORING AGENCY REPORT NUMBER NASA TM-1998-208490	
11. SUPPLEMENTARY NOTES David E. Ashpis, NASA Lewis Research Center and Eli Reshotko, Case Western Reserve University, Department of Mechanical and Aerospace Engineering, Cleveland, Ohio 44106. Responsible person, David E. Ashpis, organization code 5820, (216) 433-8317.				
12a. DISTRIBUTION/AVAILABILITY STATEMENT Unclassified - Unlimited Subject Category: 02 This publication is available from the NASA Center for AeroSpace Information, (301) 621-0390.			12b. DISTRIBUTION CODE Distribution: Nonstandard	
13. ABSTRACT (Maximum 200 words) This report documents the full details of the condensed journal article by Ashpis & Reshotko (JFM, 1990) entitled "The Vibrating Ribbon Problem Revisited." A revised formal solution of the vibrating ribbon problem of hydrodynamic stability is presented. The initial formulation of Gaster (JFM, 1965) is modified by application of the Briggs method and a careful treatment of the complex double Fourier transform inversions. Expressions are obtained in a natural way for the discrete spectrum as well as for the four branches of the continuous spectra. These correspond to discrete and branch-cut singularities in the complex wave-number plane. The solutions from the continuous spectra decay both upstream and downstream of the ribbon, with the decay in the upstream direction being much more rapid than that in the downstream direction. Comments and clarification of related prior work are made.				
14. SUBJECT TERMS Hydrodynamic instability; Transition; Boundary layers; Continuous spectra; Discrete spectra			15. NUMBER OF PAGES 59	
			16. PRICE CODE A04	
17. SECURITY CLASSIFICATION OF REPORT Unclassified	18. SECURITY CLASSIFICATION OF THIS PAGE Unclassified	19. SECURITY CLASSIFICATION OF ABSTRACT Unclassified	20. LIMITATION OF ABSTRACT	